Dynamics of the twostep photodissociation of azomethane

B. Kim Andrews, Katherine A. Burton, and R. Bruce Weisman

Citation: The Journal of Chemical Physics **96**, 1111 (1992); doi: 10.1063/1.462197
View online: http://dx.doi.org/10.1063/1.462197
View Table of Contents: http://scitation.aip.org/content/aip/journal/jcp/96/2?ver=pdfcov
Published by the AIP Publishing

Dynamics of the two-step photodissociation of azomethane

B. Kim Andrews, Katherine A. Burton,[a] and R. Bruce Weisman
Department of Chemistry and Rice Quantum Institute, Rice University, Houston, Texas 77251

(Received 7 August 1991; accepted 7 October 1991)

Time-resolved coherent anti-Stokes Raman spectroscopy (CARS) measurements have revealed aspects of energy disposal in the 355 nm photodissociation of gas phase azomethane. Interpretation of these results is aided by earlier experiments that kinetically resolved the two steps of dissociation leading to two methyl radicals and a nitrogen molecule. Methyl radicals were observed with zero to four quanta of vibrational excitation in the ν_2 out-of-plane deformation mode. Kinetic analysis showed the first-step methyl radicals to carry far more ν_2 excitation than the second-step methyl radicals. Through simulation of band contours, a rotational temperature was estimated for the vibrationally unexcited second-step methyls. In addition, nascent vibrational and rotational populations were determined for the nitrogen photoproduct, which is formed in the second dissociative step. These experimental findings are compared to the results of impulsive and statistical models of energy partitioning in this system. It appears that the first step may have significant impulsive character. In the second step, some experimental findings are predicted accurately by the separate statistical ensemble (SSE) model, while other findings fall outside the range spanned by the impulsive and SSE predictions. It is suggested that the second-step energy distributions may reflect the effects of specific exit channel interactions superimposed on statistical partitioning of available energy. Quantum chemical computations on the second step's reaction path (leading from the methyldiazenyl radical intermediate to the methyl radical and nitrogen photoproducts) should permit deeper understanding of the dissociation dynamics.

INTRODUCTION

The azoalkanes (R–N = N–R′) are a sizeable class of compounds that share a tendency to dissociate into alkyl radicals and N_2 when heated or exposed to ultraviolet light. This property makes them a popular, clean source of free radicals in organic chemistry. An azoalkane is termed symmetrical if its R and R′ substituents are the same; otherwise, it is unsymmetrical. Most azoalkanes lack direct bonding between the R and R′ groups and are therefore classified as acyclic rather than cyclic. Among the symmetrical acyclic azoalkanes, the simplest is called azomethane, CH_3–N = N–CH_3. During the 64 years since Ramsperger first reported thermal and photodissociation of azomethane vapor,[1] hundreds of published papers have addressed the mechanisms of azoalkane dissociation.[2] One basic and very persistent question was posed in 1929:[3] Do the two C–N bonds break in one step or in two? For the case of gas phase photodissociation, time-resolved coherent anti-Stokes Raman spectroscopy (CARS) has recently provided a definitive answer. CARS measurements of the appearance kinetics of all primary photofragments formed after 355 nm sample excitation directly revealed two-step dissociation in an unsymmetrical azoalkane[4] and also, most recently, in azomethane itself.[5] The following scheme summarizes azomethane's photodissociation kinetics under collisional conditions:

$$CH_3NNCH_3^* \xrightarrow{>10^9\ s^{-1}} CH_3NN\cdot + CH_3\cdot,$$

$$CH_3NN\cdot \xrightarrow{1.9\times10^8\ s^{-1}} CH_3\cdot + N_2.$$

[a] Present Address: Naval Research Laboratory, Code 6111, Washington, D.C. 20375.

Important issues still need to be resolved. One of these is the very basic question of which electronic state of azomethane undergoes the first step of dissociation. Another area of ignorance surrounds the entire class of alkyldiazenyl radicals (R–N = N·), including methyldiazenyl (CH_3–N = N·), the crucial intermediate in azomethane's stepwise photodissociation mechanism. Although aromatic diazenyl radicals are known from electron-spin resonance (ESR) studies,[6] no alkyldiazenyl has yet been observed spectroscopically despite the fact that these radicals are isoelectronic with familiar acyl radicals such as $CH_3CO\cdot$. Methyldiazenyl therefore represents an intriguing class of radicals whose structure, stability, and dissociative properties are virtually unknown. By extending azomethane photodissociation studies into the realm of reaction dynamics, it may be possible to gain new insights into the two dissociative steps and new knowledge of the dissociating species.

Two factors help to make this approach feasible. First, gas phase azomethane dissociates with unit quantum yield following near-ultraviolet excitation to its lowest excited singlet state. The photochemically relevant potential energy surfaces are therefore low lying, few in number, and suitable targets for advanced *ab initio* quantum chemical calculations. This computational accessibility permits the combined use of experiment and theory in deciphering azomethane's photochemistry, an approach not often possible for systems of this size. The second favorable aspect of azomethane is that its photoproducts, methyl radicals and nitrogen, are well-studied species whose nascent spectra can provide detailed information about internal state distributions and energy disposal. To the extent that these energy disposal patterns are characteristic of the dissociating species and their potential surfaces, one can hope to address the remaining

questions about azomethane's photochemical pathways.

In this paper, we report the results of time-resolved CARS experiments that detect the nitrogen and methyl radical fragments produced from the 355 nm photolysis of gas phase azomethane. Except for the nitrogen vibrational distribution reported earlier from this laboratory,[7] these measurements comprise the most direct dynamical information available for a dissociating azoalkane. The data on nascent product state distributions are interpreted through comparison with impulsive and statistical calculations of energy disposal.

EXPERIMENTAL METHODS

The apparatus used for time-resolved CARS measurements is shown schematically in Fig. 1. Selected pressures of azomethane and helium buffer were admitted to the static 50 cm long glass sample cell and allowed to mix by diffusion. Gas pressures were measured using capacitance manometers. All data were obtained at cell temperatures of 295 ± 2 K.

Photolysis was initiated by a 355 nm third-harmonic pulse from the Q-switched Nd:YAG laser excitation laser. This wavelength falls within azomethane's diffuse near-ultraviolet absorption band, which is assigned to the lowest $^1n,\pi^*$ transition and whose peak molar extinction coefficient is approximately $5\ M^{-1}\ cm^{-1}$.[8] Typical excitation pulse energies of 11 mJ photolyzed approximately 15% of the sample molecules located in the small probed volume within the cell.

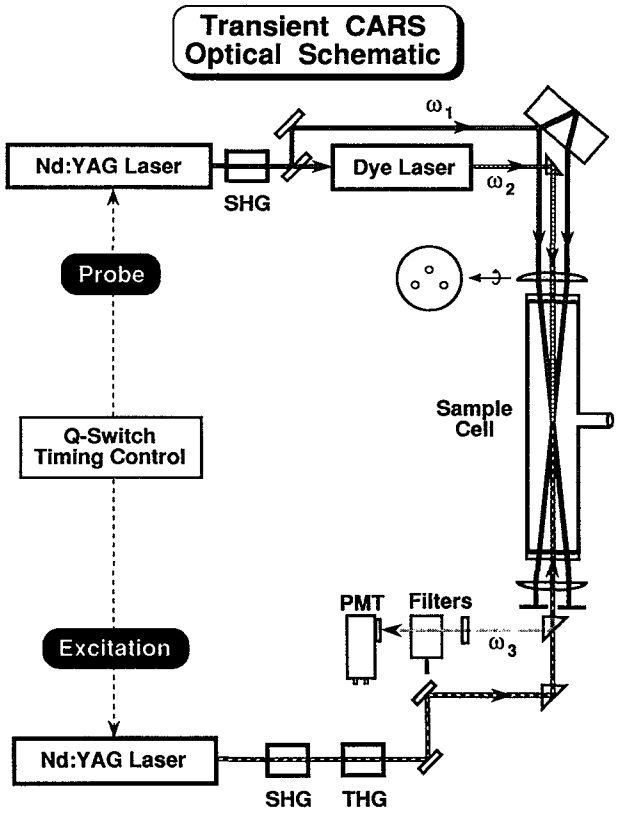

FIG. 1. An optical schematic diagram of the time-resolved CARS apparatus. SHG and THG denote nonlinear crystals used for second- and third-harmonic generation.

Following a computer-controlled electronic time delay, a separate Q-switched Nd:YAG/dye laser system generated the two beams needed to probe the CARS susceptibility of the excited sample volume. Because the CARS process is quite sensitive to spatial beam quality, the probing Nd:YAG oscillator was configured to give a near-TEM_{00} laser output. The probing YAG beam was amplified and frequency doubled, after which the 532 nm second harmonic beam was split into two portions. One of these portions was used as the fixed-frequency CARS beam (ω_1), while the other pumped a homemade three-stage dye laser, operated with DCM or Rhodamine 640 dye, whose output was the tunable CARS beam (ω_2).

As illustrated in Fig. 1, the excitation and probing beams entered opposite ends of the sample cell through uncoated fused silica windows. Phase matching of the CARS beams was achieved using the "folded BOXCARS" optical configuration in which the ω_1 beam was split into two equally intense parallel beams. After passing through a 35 cm f.l. focusing lens these replica beams crossed in a horizontal plane at the center of the sample cell. The single ω_2 probe beam entered the focusing lens slightly above the ω_1 beams and intersected them at the cell center while traveling downward in a vertical plane. The CARS process generated a new beam at frequency $\omega_3 = 2\omega_1 - \omega_2$ that emerged from the overlap region propagating upward relative to the ω_1 beams. Although the noncollinearities were smaller than one degree, they were sufficient to separate the probe beams at the cell windows and thereby prevent excessive nonresonant background generation. In addition, the noncollinear geometry permitted us to spatially filter the ω_3 light from the ω_1 and ω_2 beams, which were as much as 14 orders of magnitude more intense. In order to measure the ω_3 CARS signal intensity without contamination from residual ω_1 and ω_2 light, it was also necessary to place sharp-edge dielectric filters and a tunable grating filter in front of the Hamamatsu R1477 detection photomultiplier (PMT). The PMT charge pulse representing the ω_3 signal was collected with a gated integrator circuit card, digitized, and then processed by a specialized data acquisition program running on an LSI-11/73 lab computer. Several diagnostic photodiodes and associated gated integrators let us monitor the energies of excitation and probing beams and normalize measured CARS signals to shot-to-shot variations in the laser energies. Angular alignment of the ω_1, ω_2, and excitation beams was critical at the level of 10 arcseconds.

Repetitive CARS measurements were made at the 10 Hz repetition rate of the laser systems. CARS signals obtained from the irradiated sample volume contain components from both unexcited and excited species. To distinguish these components, the time delay separating excitation and probe pulses was alternated between positive and negative values. Negative-delay signals gave the unexcited component and the difference between positive- and negative-delay signals gave the excitation-induced CARS component. We measured time-resolved spectra by setting the positive delay to the desired value and scanning ω_2, the frequency of

the probe dye laser. The Raman shifts corresponding to these CARS signals were given by $\omega_1 - \omega_2$.

Immediately after each laser shot, photolysis reduced the concentration of azomethane and increased the concentration of photoproducts within the irradiated volume. These concentrations were restored nearly to preexisting levels by diffusion between excited and unexcited regions of the sample cell during the 100 ms interval between shots. After $\sim 10^4$ excitation pulses, the cell's overall azomethane concentration became significantly reduced and an inconveniently large amount of N_2 accumulated. The cell was then evacuated and recharged with a fresh sample. When acquiring transient N_2 spectra, it was necessary to compensate properly for background signals arising from nitrogen that had accumulated in the cell from earlier shots. Because the ω_3 CARS intensity varies quadratically with the resonant species' cross section and concentration, we subtracted the square root of the negative-delay signal from the square root of the positive-delay signal to obtain an effective Raman spectrum of the newly generated nitrogen molecules. A different data reduction method was used for measuring transient spectra of methyl radicals, because there was no accumulation of these reactive radicals from shot to shot and the negative-delay signals were dominated by weak nonresonant backgrounds. Our spectra in the C–H stretching region were obtained by taking the square root of the difference between positive- and negative-delay signals. None of the species involved in this study have electronic absorptions close to the CARS wavelengths, so the measured signals were unaffected by electronic resonance enhancement.

The instrumental time response of our apparatus was approximately 8 ns (before deconvolution) and its spectral resolution was 0.25 cm^{-1} with a line-narrowing etalon inserted in the probe YAG oscillator or 1 cm^{-1} without the etalon.

EXPERIMENTAL RESULTS

Experiments that expose samples to intense laser radiation may give misleading results because of unintended multiple photon excitation. We note that the present experimental conditions are comparable to those of earlier azomethane kinetic studies that were checked carefully and found to be free of significant multiphoton artifacts.[5]

Nitrogen vibrational distribution

We assessed the nascent vibrational distribution of the N_2 photoproducts from time-resolved spectra taken at a delay of 15 ns in samples containing 2 Torr of azomethane mixed with 400 Torr of helium buffer gas. Under these conditions, the probed nitrogen molecules have undergone approximately 80 hard sphere collisions with helium. This number may be compared with the collision numbers reported for the relaxation of nitrogen by helium: $Z_{rot} = 6$ and $Z_{vib} = 10^8$.[9] It is clear that at the time of probing, the nitrogen photoproduct should be rotationally thermalized and vibrationally nascent.

Nitrogen bands corresponding to $v = 0 \rightarrow 1$, $v = 1 \rightarrow 2$, and $v = 2 \rightarrow 3$ fundamental transitions are easily distinguished because anharmonicity separates them by 28 cm^{-1}, an interval greater than the widths of the thermalized Q branches that we observe in CARS probing. We found relative vibrational populations N_v from scans of induced square root CARS signals in which each of the dispersively shaped band origins has been evaluated for the difference between its maximum and minimum values.[10] This net signal $S_{v,v+1}$ is described by the relation

$$S_{v,v+1} = C\,|N_v - N_{v+1}|\,\sigma_{v,v+1},$$

where C is a constant and $\sigma_{v,v+1}$ is the Raman cross section for the fundamental transition between levels v and $v+1$. In analyzing the $S_{v,v+1}$ data to deduce values of N_v, we assume that $\sigma_{v,v+1}$ is proportional to $v+1$, as is true for a harmonic oscillator.[11] In addition, because no transient bands were detectable beyond $v = 2 \rightarrow 3$ and the observed band shapes indicate a normal, rather than inverted distribution, we have assumed N_3 to be zero. The nascent population distribution found from this analysis is $86 \pm 3\%$ in $v = 0$; $13 \pm 3\%$ in $v = 1$; $1 \pm 1\%$ in $v = 2$. We note that these values agree within experimental uncertainty with earlier measurements from this laboratory.[7] The average vibrational energy corresponding to this distribution is 350 ± 90 cm^{-1} per nitrogen molecule.

Nitrogen rotational distribution

The nascent rotational distribution of the N_2 photoproduct was found from the induced square root CARS spectrum of the $v = 0 \rightarrow 1$ Q branch measured with our higher resolution under unrelaxed conditions. Figure 2 shows such data taken at 5 ns delay in a sample of 2 Torr of azomethane. A notable feature of this spectrum is the negative-going depletion evident for J values below 8. It is clear that a significant number of preexisting nitrogen molecules (formed from earlier shots) have been removed from the probed volume even though the probe delay is small compared to the mean collision time of 43 ns estimated for thermalized nitrogen molecules in 2 Torr of azomethane. We presume that depletion occurs as translationally excited photoproducts

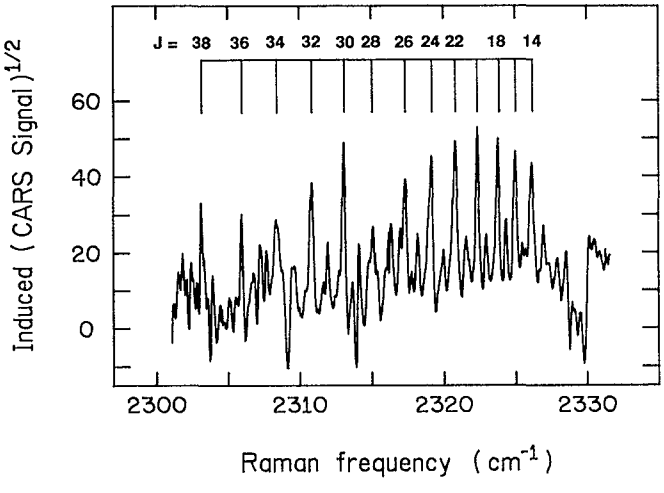

FIG. 2. The CARS spectrum of the rotationally unrelaxed N_2 photoproduct in the Q branch of the $v = 0 \rightarrow 1$ band.

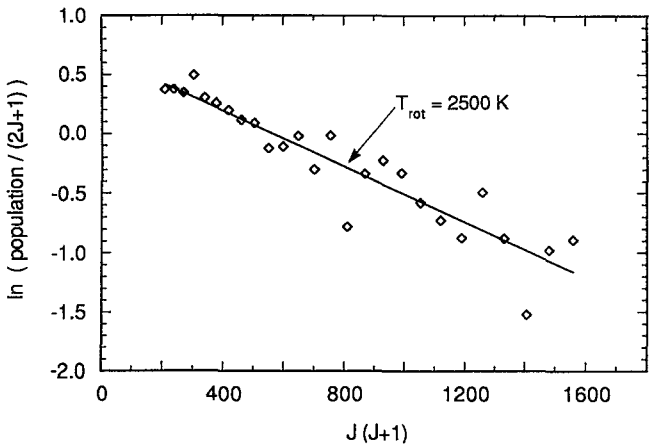

FIG. 3. The Boltzmann plot of the N_2 rotational data from Fig. 2. The solid line shows a best-fit Boltzmann distribution with $T = 2500$ K.

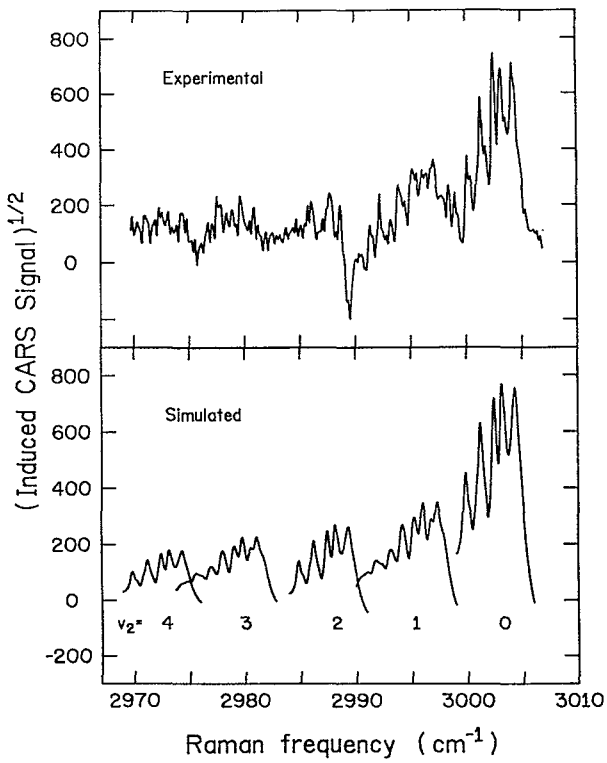

FIG. 4. Top: Induced CARS spectrum in the ν_1 fundamental region of methyl radical photofragments. The spectrum was obtained 25 ns after excitation in a sample containing 5 Torr of azomethane plus 270 Torr of helium to induce rotational thermalization. The negative-going feature at 2989 cm^{-1} results from depletion of an azomethane ground state band. Bottom: Spectral simulation with the bands labeled according to the number of quanta in the ν_2 mode.

transfer kinetic energy to background nitrogen molecules, causing some fraction of them to quickly leave the probed volume. Our data reveal the relative populations only of those rotational states whose thermal populations are small enough that their depletion has a negligible effect on the induced spectrum. This accessible range includes J values of 14 and greater. The raw induced spectra also show a negative-going pedestal corresponding to a depleted nonresonant background. To correct for this offset, we have adjusted the zero of the raw induced spectrum until the ratio of adjacent J_{even} to J_{odd} line strengths matches the 2:1 population ratio known to arise from $I = 1$ nuclear spin statistics in $^{14}N_2$.

The strengths of Q-branch lines in Fig. 2 directly provide the relative populations of corresponding rotational levels. Measurements made with the azomethane pressure reduced to 1 Torr or with probe delays set to 3 or 8 ns gave rotational distributions in good agreement with the 2 Torr, 5 ns data of Fig. 2. This agreement indicates that the measured nitrogen rotational distribution is essentially nascent and unaffected by collisions. Figure 3 shows the deduced distribution as a Boltzmann plot, in which the population of each rotational level is divided by its $2J + 1$ degeneracy factor and the logarithm of the result is plotted against $J(J + 1)$, whose value is very nearly proportional to rotational energy. A straight line on such a plot corresponds to a thermal rotational distribution. From the fit drawn in Fig. 3, it can be seen that our data are well described by a temperature of approximately 2500 K. This value differs significantly from an earlier 425 K estimate that was based on lower resolution data obtained at longer delays and higher pressures.[7] We think it likely that the previous results were seriously distorted by collisional relaxation and that the new value of 2500 K is far more reliable.

Methyl vibrational distributions

The experimental task of determining methyl product state distributions is complicated by the fact that azomethane produces a methyl radical in both of its photodissociation steps. We seek to measure not only the overall methyl excitations, but also the underlying distributions from the first and second formation steps.

Under conditions of incomplete vibrational relaxation, we observe several transient CARS bands with Raman shifts near 3000 cm^{-1}, as shown in the top frame of Fig. 4. A proper spectroscopic assignment of these bands is needed to deduce product state distributions. Our assignment begins by recognizing those features above ~ 2999 cm^{-1} as the fundamental ($v = 0 \rightarrow 1$) ν_1 band of fully thermalized methyl radicals, whose CARS spectrum was reported earlier from this laboratory.[12] The observed structure is the partly resolved rotational contour of the planar radical's $\Delta J = 0$, $\Delta K = 0$ Q branch. Spectral simulation provides the following values for the changes in rotational constants that accompany the ν_1 vibrational transition: $\Delta B = -0.086 \pm 0.001$ cm^{-1} and $\Delta C = -0.051 \pm 0.001$ cm^{-1}. These values agree well with those reported previously.[12]

Unlike the highest frequency band described above, the lower frequency spectral features of Fig. 4 are observed to vanish under vibrationally relaxed conditions. On this basis, we identify them as hot bands of the methyl radical. The proximity of these bands to the fundamental ν_1 band and the similar intervals between them suggest that they form a sequence of $\Delta v_1 = 1$ transitions that are anharmonically shifted by excitation in one of the four vibrational modes of the

TABLE I. Fundamental symmetric stretching bands of the methyl radical.

Quanta in ν_2 mode[a]	Energy in ν_2 mode[b]	Observed ν_1 band origin[c]	Frequency shift[d]	Deduced ΔB[e]	Deduced ΔC[e]	Relative population
0	0	3004.8	0	−0.086	−0.051	0.42 ± 0.06
1	606	2998.0	−6.8	−0.070	−0.060	0.20 ± 0.04
2	1288	2989.8	−15	···	···	0.15 ± 0.04
3	2019	2980.8	−24	···	···	0.13 ± 0.03
4	2790	2974.8	−30	···	···	0.10 ± 0.03

[a] ν_2 is the A_2'' out-of-plane deformation vibration.
[b] In cm^{-1}, based on data of Ref. 33 and C. Yamada, E. Hirota, and K. Kawaguchi, J. Chem. Phys. **75**, 5256 (1981).
[c] In cm^{-1}, for the ν_1 fundamental transition, with estimated uncertainties of 0.2 cm^{-1}.
[d] In cm^{-1}, relative to the $\nu_2 = 0$ band origin.
[e] In cm^{-1}, based on spectral simulation of CARS band contours.

methyl radical. Which is the excited mode that gives this sequence? We can rule out ν_1 itself because the observed intervals are far smaller than the 45.4 cm^{-1} value found from resonance Raman scattering.[13] Two observations point instead to ν_2, the out-of-plane deformation, as the sequence mode. First, the average spacing seen in our data is ~ -7.5 cm^{-1}, a result reasonably close to methyl's reported X_{12} anharmonic constant of -9.8 cm^{-1} (Ref. 13) and consistent with the -5 cm^{-1} value deduced for X_{12} of CD_3.[14] The second piece of evidence comes from our spectral simulation of the first hot band's rotational contour. Fermi statistics requires that the D_{3h} methyl radical's total wave function change sign upon interchange of any two H nuclei, a condition that imposes A_2 rotational subgroup symmetry on the direct product $\Gamma_{el} \otimes \Gamma_{vib} \otimes \Gamma_{rot} \otimes \Gamma_{spin}$.[15] In the vibrationless ground electronic state of CH_3, $\Gamma_{el} \otimes \Gamma_{vib}$ is $A_2 \otimes A_1 = A_2$ and the product $\Gamma_{rot} \otimes \Gamma_{spin}$ must therefore equal A_1. This leads to a characteristic pattern of nuclear spin statistical weights for methyl's symmetric rotor levels—2 for $K = 0$ and even J; 0 for $K = 0$ and odd J; 2 for $K = 3q$ (with q a nonzero integer); and 1 for $K = 3q \pm 1$. Although these spin weights allow successful modeling of the cold ν_1 band contour, they are less satisfactory for the first hot sequence band. Instead, we obtain better agreement with experiment using spin weights that correspond to A_2'' vibrational symmetry—0 for $K = 0$ and even J; 2 for $K = 0$ and odd J; 2 for $K = 3q$ (with q a nonzero integer); and 1 for $K = 3q \pm 1$. Evidently then, one quantum of vibrational excitation makes the methyl radical's vibrational symmetry A_2'', and the excited mode can only be ν_2. We conclude that the transient CARS bands near 3000 cm^{-1} correspond to $v_1 = 0 \rightarrow 1$ transitions in methyl radicals that have zero, one, two, three, or four quanta of excitation in their out-of-plane ν_2 mode, as labeled in the bottom frame of Fig. 4. Table I summarizes the relevant data for these bands.

The band amplitudes in Fig. 4 provide the basis for determining relative ν_2 populations of the nascent methyl photofragments. First, we note that the helium buffer gas added to the sample collapses the rotational band contours to the point that they are nearly nonoverlapping, without significantly affecting the relative vibrational populations. Then, with the expectation that the Raman cross section of methyl's fundamental ν_1 transition is nearly independent of ν_2 excitation, we obtain relative ν_2 populations relative directly from the band amplitudes. The last column of Table I shows the resulting deduced ν_2 distribution, representing the sum of first-step and second-step methyl photofragments. To determine the subdistributions for the two types of methyl radicals, we rely on CARS kinetic data of the type that was earlier used to link the cold band mainly with second-step methyl and the first hot band mainly with first-step methyl.[5] From detailed kinetic analysis, we estimate that 10% ± 5% of the $v_2 = 0$ population is formed in the first dissociative step and 15% ± 5% of the $v_2 = 1$ population is formed in the second step. Although the quality of our kinetic data does not support such an analysis for the other hot bands, it seems likely that they contain an even smaller contribution from second-step methyls. Our deduced distributions of ν_2 excitation in the first-step, second-step, and overall methyl radical populations are graphed in Fig. 5.

To assess the population of methyl photofragments excited in their ν_1 (symmetric C–H stretching) mode, we searched for CARS transients near 2957 cm^{-1}. This is the frequency at which $v_1 = 1 \rightarrow 2$ transitions are expected, based on the location of the (cold) $v_1 = 0 \rightarrow 1$ band and the 22.7 cm^{-1} value reported for methyl's X_{11} anharmonicity constant.[13] No transient bands were detected in this region, and from our noise level we conclude that less than 10% of

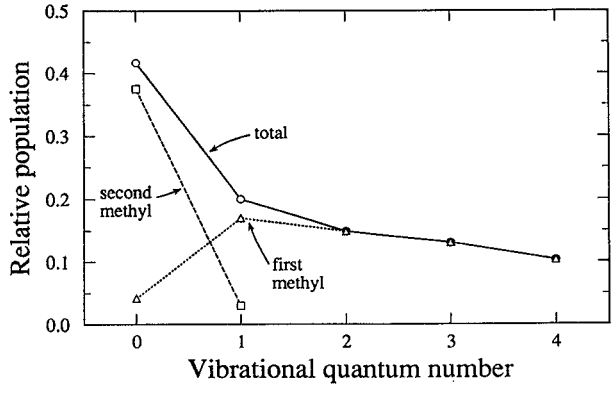

FIG. 5. Nascent ν_2 population distributions deduced for the methyl radicals formed in 355 nm photolysis of azomethane vapor. The population in $v = 2$, 3, and 4 has been assigned to the first methyl radical by assumption.

TABLE II. Energy disposal in 355 nm photolysis of azomethane.[a]

		First step		Second step	
Component	Model	Methyl	Methyldiazenyl	Methyl	Nitrogen
Vibration	Experimental	1421[e]		45[e]	350
	Impulsive[b]	1176		621	291
	Statistical (SSE)[c]	653[e,f]	6100	770[e]	307
Rotation	Experimental			1360	1740
	Impulsive[b]	0		0	1031
	Statistical (SSE)[d]	1093	1093	1513	1009
Vibration + Rotation	Experimental				
	Impulsive[b]	1176	3382	621	1322
	Statistical (SSE)[d]	2894	7193		
Translation	Experimental				
	Impulsive[b]	4670	1631	2464	1322
	Statistical (SSE)[d]	810	283	985	529

[a]Average energy components in cm^{-1}.
[b]Available energy of 10 860 cm^{-1} for the first step; 5730 cm^{-1} for the second step.
[c]Available energy of 11 180 cm^{-1} for the first step; 5630 cm^{-1} for the second step.
[d]Available energy of 11 180 cm^{-1} for the first step; 11 420 cm^{-1} for the second step.
[e]For the ν_2 mode only.
[f]Total vibrational energy equals 1801 cm^{-1}.

the methyl photofragments are formed with one quantum of excitation in the ν_1 mode.

Methyl rotational distributions

In order to measure the unrelaxed rotational contour of methyl radical photoproducts, we took spectra of the ν_1 fundamental band at 0.25 cm^{-1} resolution in samples containing only 5 Torr of azomethane. No significant spectral differences were seen as the delay was varied from 3 to 8 ns. By performing spectral simulation of this band using appropriate spectroscopic constants and a variable temperature parameter, we found that the band contour was best described by a methyl rotational temperature of 1300 ± 200 K. Two factors contribute added uncertainty to this result. First, there may have been some collisional distortion of the rotational distribution under the conditions used. Second, although we have deduced that the fundamental band arises predominantly from second-step methyl radicals, first-step methyl radicals make some contribution to the spectrum. For these reasons, the value of 1360 cm^{-1} ($3/2\ kT_{rot}$) that we find as the average rotational energy carried by second-step methyl radicals should be viewed as tentative. Spectral overlap and lower signal-to-noise ratios prevented rotational analyses of the ν_1 sequence bands. Table II summarizes all of the average vibrational and rotational fragment energies deduced from our time-resolved spectroscopic studies of azomethane's 355 nm photodissociation.

COMPUTATIONAL METHODS AND RESULTS

Energetics

Before one can interpret patterns of energy disposal, it is necessary to know the amount of energy released during photodissociation. Absorption of a 355 nm excitation photon adds 336.9 kJ/mol (28 170 cm^{-1}) to azomethane. Reported thermochemical measurements provide the following relevant gas phase heats of formation: 148.5 kJ/mol for azomethane;[16] 143.5 kJ/mol for the methyl radical;[17] and 209.6 kJ/mol for the methyldiazenyl radical.[18,19] Using these values and adjusting for the difference between enthalpy and internal energy changes, we obtain 129.9 kJ/mol (10 860 cm^{-1}/molecule) as the energy that will appear in products of the first step of photodissociation, excluding contributions from azomethane's thermal excitation. The average thermal rotational energy of azomethane is simply $3/2\ RT$, or 2.46 kJ/mol (310 cm^{-1}/molecule) at 296 K. Its average vibrational energy content is calculated to be 3.8 kJ/mol (320 cm^{-1}/molecule) based on frequencies reported from infrared and Raman spectroscopy.[20] It seems likely that azomethane's ground state vibrational and rotational distributions are transferred into the excited state during optical excitation of the diffuse $S_1 \leftarrow S_0$ transition.

In the second step of dissociation, the energy released to products equals 63.5 kJ/mol (5320 cm^{-1}) plus the residual first-step excitation of the methyldiazenyl radical intermediate. We estimate from computed vibrational frequencies that the methyldiazenyl radical carries 310 cm^{-1} of average vibrational energy when thermalized at 296 K. Our quantum chemical calculations also show that methyldiazenyl radicals dissociate on their $^2A'$ ground potential surface over a small barrier whose energy is approximately 4.9 kJ/mol (410 cm^{-1}) above the methyldiazenyl minimum.[21] Figure 6 illustrates the basic energetics of azomethane's 355 nm photodissociation.

Energy disposal

The partitioning of available energy into rotations, vibrations, and translations of the product species is a complex process whose detailed prediction may in principle require scattering calculations on accurate potential surfaces. However, simpler treatments may adequately describe the energy

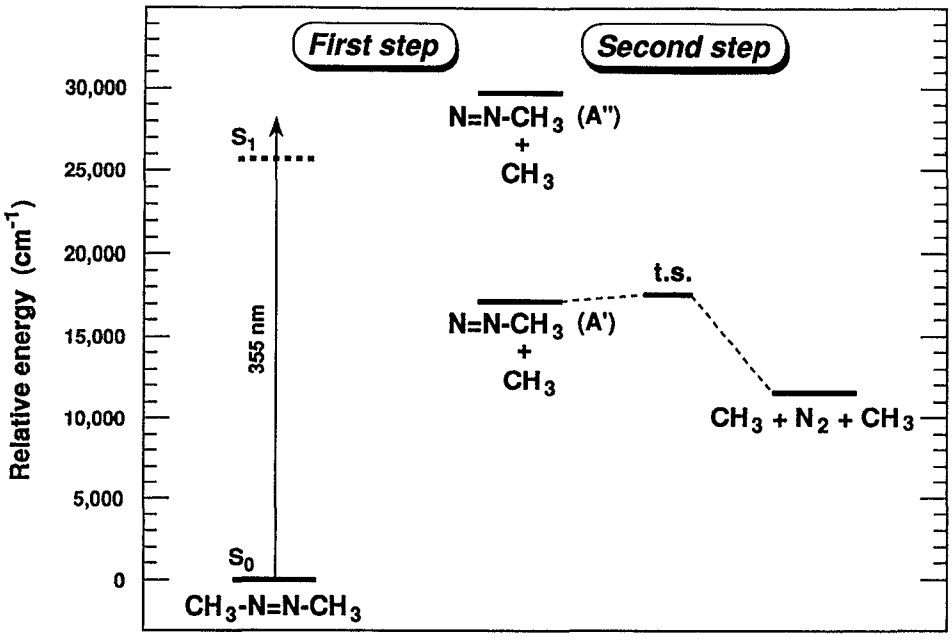

FIG. 6. Photochemical energetics of azomethane based on data discussed in the text.

disposal in certain important limits. If release of reaction energy occurs rapidly compared to the rate of energy flow in the dissociating system, then energy disposal should be governed by impulsive kinematics. In the opposite limit of energy flow that is rapid compared to bond breaking, one might expect the final energy to be partitioned so as to give a distribution with the greatest possible statistical weight. By comparing the experimental energy disposal data to the predictions of these impulsive and statistical limiting case models, we hope to gain some information about the potential energy surfaces involved in azomethane's photodissociation.

IMPULSIVE MODELS

The "impulsive" model describes reactions in which energy release is rapid compared to the rate of intramolecular energy redistribution. As presented by Busch and Wilson for triatomics,[22] reaction exoergicity appears initially as recoil kinetic energy of the two atoms linked by the breaking bond. The partitioning of this recoil energy into translational, rotational, and vibrational excitations of the photofragments is then found from simple classical kinematics, with masses and bond angles controlling the energy disposal. To apply the impulsive model to the polyatomic fragments formed from azomethane, we use the extension given by Trentelman *et al.*[23] and assume that in each step of dissociation, the (C–N bond) recoil axis passes through the methyl group's center of mass, allowing no impulsive rotational excitation of the methyl fragments.

Impulsive calculations require a parameter representing the amount of kinetic energy liberated initially as the system evolves quickly from reactants to products. This available energy parameter seems best represented by the drop in potential energy between transition state and products. For the second step of dissociation, we use 5730 cm^{-1} (5320 cm^{-1} exoergicity plus 410 cm^{-1} barrier height) for the impulsive available energy. In the first dissociation step, however, too little is known about the relevant potential energy surfaces to make such an estimate. Instead we simply use the value 10 860 cm^{-1}, the total energy available to first-step products. These impulsive energy disposal results for the first step should therefore be viewed as upper limits to impulsive results based on more detailed knowledge of azomethane surfaces. Table II shows our impulsive energy disposal predictions for both steps.

Apart from the kinematic excitations considered above, rapid dissociation can also excite fragment vibrational modes that undergo large changes in equilibrium geometry during the reaction. We have calculated such a "sudden" vibrational distribution for the N_2 photoproduct by squaring the overlap integrals between one-dimensional harmonic oscillator wave functions representing the $v = 0$ N–N stretching vibration of the methyldiazenyl radical at its dissociative transition state, and the $v = 0$, 1, and 2 states of the free N_2 molecule. Values for the equilibrium N–N separation and normal mode frequencies of the methyldiazenyl transition state were obtained from *ab initio* complete active space self-consistent field (CASSCF) calculations that will be reported separately.[21] As expected, the resulting Franck–Condon-like factors depend most sensitively on the change in equilibrium separation between the transition state and free N_2. We find that the 70 pm change predicted by the quantum chemical calculations corresponds to a nascent vibrational distribution of 35% $v = 0$, 32% $v = 1$, and 11% $v = 2$. This represents the maximum Franck–Condon excitation of the nitrogen, and to the extent that second-step dissociation is not actually rapid compared to the rate of intramolecular energy flow, a cooler distribution will result.

Using a similar computational approach, we have also found the Franck–Condon excitation that would be imparted to the methyl photofragments' ν_2 out-of-plane deformation vibration during a sudden transition from pyramidal to planar equilibrium structures. In this case, the one-dimensional harmonic oscillator wave functions represented the ν_2

mode of free CH_3 and the corresponding normal mode of the parent species. A conventional transformation from normal to Cartesian coordinates[24] allowed us to obtain the methyl radical ν_2 distribution as a function of the N–C–H bond angle at the dissociative transition state. For the second step of azomethane dissociation, our computed methyldiazenyl transition state structure has an average N–C–H angle of 105°,[21] which gives a Franck–Condon distribution with 2% in $v = 0$; 7% in $v = 1$; 14% in $v = 2$; 20% in $v = 3$; and 20% in $v = 4$. As mentioned earlier, a less energetic population distribution will result from fragmentation that is slower than "sudden." For azomethane's first dissociative step, we do not have a computed transition state geometry from which to predict the Franck–Condon ν_2 distribution of the first methyl radical. However, the prediction that most closely matches the experimental first-step ν_2 distribution corresponds to an abrupt change in the N–C–H equilibrium angle to 90° from 102°.

STATISTICAL MODELS

In the opposite limit that the intramolecular flow of energy is rapid compared to individual dissociation events, partitioning of available energy into fragment modes may be governed by statistical weights rather than dynamical effects. Descriptions of this partitioning include the prior distribution,[25,26] the statistical adiabatic channel method (SACM),[27] and the separate statistical ensemble (SSE) approach.[28] We have chosen the SSE method for calculating a statistical energy partitioning in azomethane photodissociation because of its computational simplicity and its agreement with experimental results in other systems.[29,30]

SSE calculations are based on the idea that in unimolecular reactions, vibrations of the products derive only from the $3N - 6$ reactant vibrations, not from the full set of reactant vibrations and rotations. To calculate the probability of forming a specific vibrational level of the nitrogen photoproduct, we first subtracted the energy of that level from the 5630 cm^{-1} total energy available to the second step products (including methyldiazenyl's thermalized vibrational energy). Using the scheme presented by Wittig *et al.*,[28] we then computed the number of states that could be formed by distributing this residual energy over the six methyl radical vibrations and the five unhindered (rotational and translational) product degrees of freedom that arise from reactant vibrations. The set of vibrational states was calculated using the exact state-counting Beyer–Swinehart algorithm.[31,32] The probability of forming the nitrogen vibrational level was assumed proportional to the resulting number of states, and by repeating the calculation for all energetically accessible levels, we obtained the following nitrogen vibrational distribution: 87.4% in $v = 0$; 12.1% in $v = 1$; 0.6% in $v = 2$. This agrees within experimental error with the measured nascent distribution described under Experimental Results. The average vibrational energy per nitrogen molecule is 307 cm^{-1} in this SSE calculation, considerably greater than the 180 cm^{-1} value found using a statistical prior distribution.

A similar SSE calculation for the ν_2 vibrational mode of second-step methyl radicals predicts the distribution 41% in $v = 0$; 27% in $v = 1$; 16% in $v = 2$; 9% in $v = 3$; 4% in $v = 4$; 2% in $v = 5$; and 0.7% in $v = 6$. Table II includes the corresponding average ν_2 energy of 770 cm^{-1}. Clearly, this distribution is hotter than that deduced experimentally for second step methyl radicals.

In contrast to the second-step vibrational distributions, which were measured in the presence of enough helium buffer gas to thermalize the methyldiazenyl intermediate, the nitrogen rotational populations were observed under precollisional conditions. To predict these rotational data, one therefore needs to know how much internal energy the methyldiazenyl radical has acquired from the first step of dissociation because this amount will add to the available energy in the second step. We have computed the distribution of vibrational energy imparted to methyldiazenyl in the first step using the SSE method with a set of methyldiazenyl vibrational frequencies derived from our *ab initio* quantum calculations. The resulting probability distribution has a maximum and a mean near 6100 cm^{-1} with a full width at half-maximum of 5000 cm^{-1}. The average available energy for the second step was therefore assumed to be 6100 cm^{-1} plus the 5320 cm^{-1} exothermicity, for a total of 11 420 cm^{-1}. This value for the second-step available energy was used in SSE calculations to predict nascent vibrational energy contents of the second methyl radical and nitrogen molecule, giving values of 5947 and 1438 cm^{-1}, respectively. We then assumed that the remaining 7385 cm^{-1} was distributed statistically over second-step product rotations and translations in accord with the equipartition principle. This procedure predicts the rotational and translational average energies listed in the right half of Table II, including average rotational energy contents of 1513 and 1009 cm^{-1} for the methyl radical and the nitrogen.

First-step SSE calculations of the methyl ν_2 populations were performed using the list of computed methyldiazenyl vibrational levels mentioned above. The resulting distribution has an average energy content in the methyl ν_2 mode of 653 cm^{-1}. Repeating this calculation for the full set of methyl vibrations gave 1801 cm^{-1} as the total average vibrational energy of nascent first-step methyl radicals. To obtain statistically predicted rotational and translational average energies for the first-step products, we subtracted the average methyl and methyldiazenyl vibrational energies from the 11 180 cm^{-1} of available energy and used equipartition to divide the 3279 cm^{-1} remainder among the nine unhindered degrees of freedom. In this way, the first-step products are each predicted to have 1093 cm^{-1} of average rotational energy. For comparison, a prior distribution allocates 1439 cm^{-1} to these modes.

DISCUSSION

The present results provide just a partial view of energy disposal in azomethane photolysis. Nevertheless, comparison to the limiting theoretical models allows some interesting deductions. For the first step of photodissociation, we have data only on the methyl radical's ν_2 distribution, which appears nonstatistical and slightly more than twice as energetic as SSE predicts. The impulsive model's prediction is in much better agreement here—only 17% lower than ob-

served. Nonstatistical excitation of first-step methyl radicals may be related to special properties of the ν_2 mode—it is the lowest frequency vibration of CH_3; its carbon atom displacements are nearly collinear with the breaking bond; and its motion mimics the planarization of the pyramidal methyl group as it evolves into a free radical. In the case of abrupt, impulsive energy release, the first two of these properties will cause efficient transfer of the reaction's exoergicity into ν_2 excitation.[23,33] Coupling of the vibrational mode to the reaction coordinate, the third property, may lead to nonstatistical behavior even when the release of reaction energy is not abrupt. The limited first-step data that are available to us suggest a significant impulsive character in the first step of azomethane photodissociation. Future measurements of the first-step CH_3 rotational distribution should provide an interesting check—an energy content near 1100 cm^{-1} would point to statistical partitioning, whereas low values would support the impulsive description, in which the emerging methyl radical would gain little rotational excitation because the impulse is directed nearly along its C_3 symmetry axis.

In the second step, the SSE prediction falls well within experimental error of the measured nitrogen vibrational distribution. Although the impulsive model's predicted nitrogen vibrational energy content is somewhat lower, it too falls within the experiment's uncertainty range. However, we note that because nitrogen's vibration is "stiff," an impulsive model that is otherwise appropriate will tend to overestimate disposal of energy into this mode.[22] From this viewpoint, the underestimated impulsive prediction seems less successful. A statistical prior distribution predicts an average vibrational energy too low by 49%. Even further from our experimental results (in the opposite direction) is the "sudden" vibrational distribution obtained by Franck–Condon projection of the transition state onto the free N_2 molecule. To summarize, the nitrogen vibrational data agree well with the SSE model, appear fairly consistent with a simple impulsive model, and disagree with other descriptions.

Turning to the nitrogen's rotational excitation, both the impulsive and the SSE models underestimate the mean rotational energy by about 41%. The available energy parameter used in the impulsive calculation is 5730 cm^{-1}, a value that neglects the unrelaxed methyldiazenyl excitation remaining from the first step because, in the spirit of the simple impulsive model, parent vibrational energy should not contribute to forces along the breaking bond. Admittedly, however, parent rotational motion will influence fragment rotations. Although it is not clear in this case whether parent rotation will augment or cancel the second-step rotation, an additive effect of this sort might explain the large discrepancy between the experimental nitrogen rotational energy content and the impulsive prediction.

The SSE and impulsive models give such similar nitrogen predictions that we cannot exclude either of them based on the second-step results discussed so far. However, their predicted methyl rotational energies are very different. The statistical prediction of 1513 cm^{-1} lies only 11% above the experimentally deduced energy, whereas the impulsive model allows no rotational excitation as long as the methyl group's symmetry axis stays aligned with the breaking C–N bond. Even though the vibrationally excited methyldiazenyl radical will in fact undergo serious distortions away from its aligned equilibrium structure, we interpret the substantial methyl rotational energy as evidence favoring statistical energy partitioning in the second step.

A theoretical result also supports statistical energy partitioning in the second step—the *ab initio* potential energy surface computed for methyldiazenyl along its dissociation path to N_2 and CH_3 shows only small slopes,[21] suggesting that release of reaction exoergicity will probably be slower than intramolecular energy flow. If, based on this observation and the factors discussed above, we assume that the excitation of nitrogen's vibration and methyl's rotations do reflect statistical disposal of the available energy, then how can we account for the small methyl ν_2 energy and the excess nitrogen rotational energy? One consideration is that the 45 cm^{-1} experimental ν_2 energy, which relies on a kinetic separation of the sequence bands into first- and second-step components, may be too low. Only the $v = 0$ and $v = 1$ data were quiet enough to permit this separation and we have presumed, based on the small second-step component in the $v = 1$ band, that higher ν_2 sequence bands arise entirely from first-step methyl radicals. Our 45 cm^{-1} value may therefore be viewed as a minimal estimate of the actual second-step ν_2 energy. Nevertheless, it seems that at least the $v = 1$ population is smaller than statistical for second-step methyl radicals. As a speculative explanation, one can imagine that the reaction's exoergicity is released gradually and statistically repartitioned as the methyldiazenyl radical evolves toward products, its C–N–N angle falling from 118° to smaller values. Then, out in the productlike region of the reaction path, incipient methyl radical ν_2 motion may be converted into rotational motion of both product species through a repulsive interaction between the in-plane methyl hydrogen and the end nitrogen atom. Because this conversion would occur when the fragments are nearly separated, subsequent energy redistribution might be inefficient and the exit channel effects would then appear superimposed on otherwise statistical disposal of available energy. We will defer further discussion of such interactions to a separate paper that will include detailed calculations of the second-step potential energy surface along the intrinsic reaction coordinate.[21]

Although they are not available from our data, translational energy distributions should permit a clear distinction between impulsive and statistical energy release. Figure 2 shows that the impulsive model predicts translational fragment energies greater than the SSE model's predictions by factors of 5.8 in the first step and 2.5 in the second. If a statistical prior calculation is used instead of SSE, these factors change to 4.4 and 1.6. It is interesting that in contrast to the impulsive model, SSE predicts quite similar translational energies for the first and second methyl radicals. (Note, however, that second-step translational energies refer to the reference frame of the methyldiazenyl radical, which will have a substantial laboratory velocity from first-step translational energy release.) It seems clear that further experiments aimed at measuring photoproduct translational energies will prove very valuable in complementing the results

reported here and helping to clarify azomethane's dissociation steps.

Few other molecules that undergo three-fragment photodissociation have been the subject of reaction dynamics studies. A thorough spectroscopic investigation of acetone excited at 193 nm showed energy partitioning that was described well by the simple impulsive model.[23] However, an impulsive description failed to account for the fragment energies measured in the 157.6 nm photodissociation of C_3O_2 into two CO molecules plus a carbon atom.[34] A crude statistical model enjoyed limited success in this system, but the extra complexity of multiple reaction channels leaves the dissociation dynamics unclear. Product translational energy analysis has been used to investigate dimethyl mercury[35] and *s*-tetrazine,[36] both of which also undergo three-fragment photodissociation. Within this special class of photodissociating compounds, azomethane is an appealing system for continued study because (i) its stepwise fragmentation has been clearly established; (ii) the two steps may illustrate different forms of energy disposal; (iii) its reaction intermediate and products can be formed only in their ground electronic states; and (iv) realistic potential surfaces can be computed to help interpret experimental findings.

CONCLUSIONS

Time-resolved CARS measurements have provided a first view of the stepwise photodissociation dynamics of gas phase azomethane. For the first step, our only relevant observation is a greater-than-statistical ν_2 "umbrella" excitation in the methyl radical, suggesting the importance of impulsive effects. For the second step, we find that neither the statistically based SSE method nor the simple impulsive model can account for all of the data. However, SSE gives good predictions for the nitrogen vibrational distribution and for the methyl rotational energy. The experimental second-step methyl ν_2 excitation is anomalously low and the nitrogen rotational energy, anomalously high. We suggest that second-step energy disposal may reflect specific exit channel interactions superimposed on otherwise statistical partitioning.

Many questions about azomethane's photodissociation remain unanswered. To gain a more complete view of energy disposal patterns, additional spectroscopic measurements of the methyl rotational distributions will be valuable.[37] In addition, measurements of photoproduct translational energies may prove decisive in testing the competing theoretical models. It currently appears feasible to correlate azomethane's second-step dynamics with features of the corresponding potential surface. However, a similar understanding of the first step of photodissociation will require more experimental and computational work to identify the dissociating azomethane potential surface and characterize the path to methyldiazenyl and methyl radicals. Because second-step fragmentation can depend on the energy deposited into the methyldiazenyl intermediate in the first step, progress in clarifying the first step will benefit studies of the second. Finally, the methyldiazenyl radical is itself a deserving subject for spectroscopic as well as computational study.

ACKNOWLEDGMENTS

We thank J. S. Adams and P. S. Engel for helpful discussions and sample preparation. This research was supported by the National Science Foundation and the Robert A. Welch Foundation. Computational facilities were provided by NSF instrumentation Grant No. CHE-8909777.

[1] H. C. Ramsperger, J. Am. Chem. Soc. **49**, 912 (1927).
[2] For a review, see P. S. Engel, Chem. Rev. **80**, 99 (1980).
[3] H. C. Ramsperger, J. Am. Chem. Soc. **51**, 2134 (1929).
[4] J. S. Adams, K. A. Burton, B. K. Andrews, R. B. Weisman, and P. S. Engel, J. Am. Chem. Soc. **108**, 7935 (1986).
[5] K. A. Burton and R. B. Weisman, J. Am. Chem. Soc. **112**, 1804 (1990).
[6] T. Suehiro, Rev. Chem. Intermed. **10**, 101 (1988).
[7] P. L. Holt, K. E. McCurdy, J. S. Adams, K. A. Burton, R. B. Weisman, and P. S. Engel, J. Am. Chem. Soc. **107**, 2180 (1985).
[8] S. S. Collier, D. H. Slater, and J. G. Calvert, Photochem. Photobiol. **7**, 737 (1968).
[9] J. D. Lambert, *Vibrational and Rotational Relaxation in Gases* (Clarendon, Oxford, 1977).
[10] S. A. Druet and J.-P. E. Taran, Prog. Quantum Electron. **7**, 1 (1981).
[11] D. A. Long, *Raman Spectroscopy* (McGraw–Hill, New York, 1977).
[12] P. L. Holt, K. E. McCurdy, R. B. Weisman, J. S. Adams, and P. S. Engel, J. Chem. Phys. **81**, 3349 (1984).
[13] P. B. Kelly and S. G. Westre, Chem. Phys. Lett. **151**, 253 (1988).
[14] J. T. Miller, K. A. Burton, R. B. Weisman, W.-X. Wu, and P. S. Engel, Chem. Phys. Lett. **158**, 179 (1989).
[15] G. Herzberg, *Molecular Spectra and Molecular Structure* (Van Nostrand–Reinhold, New York, 1945), Vol. 2, Chaps. 1 and 4.
[16] P. S. Engel, R. L. Montgomery, M. Mansson, R. A. Leckonby, H. L. Foyt, and F. D. Rossini, J. Chem. Thermodyn. **10**, 205 (1978).
[17] S. W. Benson, *Thermochemical Kinetics*, 2nd ed. (Wiley, New York, 1976).
[18] P. S. Engel, J. L. Wood, J. A. Sweet, and J. L. Margrave, J. Am. Chem. Soc. **96**, 2381 (1974).
[19] G. Acs and A. Peter, Int. J. Chem. Kinet. **19**, 929 (1987).
[20] N. C. Craig, M. N. Ackermann, and R. A. MacPhail, J. Chem. Phys. **68**, 236 (1978).
[21] B. K. Andrews and R. B. Weisman (to be published).
[22] G. E. Busch and K. R. Wilson, J. Chem. Phys. **56**, 3626 (1972).
[23] K. A. Trentelman, S. H. Kable, D. B. Moss, and P. L. Houston, J. Chem. Phys. **91**, 7498 (1989).
[24] S. Silver and W. H. Shaffer, J. Chem. Phys. **9**, 599 (1941).
[25] J. L. Kinsey, J. Chem. Phys. **54**, 1206 (1971).
[26] R. D. Levine and R. B. Bernstein, *Molecular Reaction Dynamics and Chemical Reactivity* (Oxford, New York, 1987).
[27] M. Quack and J. Troe, Int. Rev. Phys. Chem. **1**, 97 (1981).
[28] C. Wittig, I. Nadler, H. Reisler, M. Noble, J. Catanzarite, and G. Radhakrishnan, J. Chem. Phys. **83**, 5581 (1985).
[29] C. X. W. Qian, M. Novle, I. Nadler, H. Reisler, and C. Wittig, J. Chem. Phys. **83**, 5573 (1985).
[30] S. K. Kim, Y. S. Choi, C. D. Pibel, Q.-K. Zheng, and C. B. Moore, J. Chem. Phys. **94**, 1954 (1991); W. H. Green, Jr., A. J. Mahoney, Q.-K. Zheng, and C. B. Moore, J. Chem. Phys. **94**, 1961 (1991).
[31] T. Beyer and D. F. Swinehart, Commun. Assoc. Comput. Machin. **16**, 379 (1973).
[32] S. E. Stein and B. S. Rabinovitch, J. Chem. Phys. **58**, 2438 (1973).
[33] H. W. Hermann and S. R. Leone, J. Chem. Phys. **76**, 4766 (1982).
[34] C. E. M. Strauss, S. H. Kable, G. K. Chawla, P. L. Houston, and I. R. Burak, J. Chem. Phys. **94**, 1837 (1991).
[35] C. F. Yu, F. Youngs, K. Tsukiyama, R. Bersohn, and J. Preses, J. Chem. Phys. **85**, 1382 (1986).
[36] X. Zhao, W. B. Miller, E. J. Hintsa, and Y. T. Lee, J. Chem. Phys. **90**, 5527 (1989).
[37] See, for example, G. E. Hall, D. Vanden Bout, and T. J. Sears, J. Chem. Phys. **94**, 4182 (1991).